ARMY RESEARCH LABORATORY

Near-room-temperature Mid-infrared Photoconductor Signal and Noise Characterization

by Justin R. Bickford, Neal K. Bambha, and Wayne H. Chang

ARL-TR-6169 **September 2012**

NOTICES

Disclaimers

The findings in this report are not to be construed as an official Department of the Army position unless so designated by other authorized documents.

Citation of manufacturer's or trade names does not constitute an official endorsement or approval of the use thereof.

Destroy this report when it is no longer needed. Do not return it to the originator.

Army Research Laboratory
Adelphi, MD 20783-1197

ARL-TR-6169 **September 2012**

Near-room-temperature Mid-infrared Photoconductor Signal and Noise Characterization

Justin R. Bickford, Neal K. Bambha, and Wayne H. Chang
Sensors and Electron Devices Directorate, ARL

REPORT DOCUMENTATION PAGE

Form Approved
OMB No. 0704-0188

1. REPORT DATE *(DD-MM-YYYY)*	2. REPORT TYPE	3. DATES COVERED (From - To)
September 2012	Final	28 August 2012

4. TITLE AND SUBTITLE
Near-room-temperature Mid-infrared Photoconductor Signal and Noise Characterization

5a. CONTRACT NUMBER

5b. GRANT NUMBER

5c. PROGRAM ELEMENT NUMBER

6. AUTHOR(S)
Justin R. Bickford, Neal K. Bambha, and Wayne H. Chang

5d. PROJECT NUMBER
KEAPS & PICS

5e. TASK NUMBER

5f. WORK UNIT NUMBER

7. PERFORMING ORGANIZATION NAME(S) AND ADDRESS(ES)
U.S. Army Research Laboratory
ATTN: RDRL-SEE-E
2800 Powder Mill Road
Adelphi, MD 20783-1197

8. PERFORMING ORGANIZATION REPORT NUMBER
ARL-TR-6169

9. SPONSORING/MONITORING AGENCY NAME(S) AND ADDRESS(ES)
CERDEC I2WD-Futures Branch
ATTN: Charles Kaiser
Aberdeen Proving Ground, MD 21005

ARDEC Fuze Division
ATTN: Nick Cali
Picatinny Arsenal, NJ 07806

10. SPONSOR/MONITOR'S ACRONYM(S)

11. SPONSOR/MONITOR'S REPORT NUMBER(S)

12. DISTRIBUTION/AVAILABILITY STATEMENT
Approved for public release; distribution unlimited.

13. SUPPLEMENTARY NOTES

14. ABSTRACT
Uncooled mid-infrared photoconductors are used in situations where hot objects (such as fire, explosions, engines, etc.) need to be detected using compact, low-cost systems. We have experienced trouble obtaining reliable detector data from mid-infrared photoconductor vendors. The purpose of this report is to give a detailed discussion of how to characterize the signal and noise properties of photodetectors with an emphasis on avoiding the measurement pitfalls associated specifically with room temperature and near room temperature mid-infrared photoconductors. The report ends with a discussion of where it is appropriate to use a commonly used figure of merit.

15. SUBJECT TERMS
PICS, KEAPS, MIR photoconductor, measurement and analysis

16. SECURITY CLASSIFICATION OF:			17. LIMITATION OF ABSTRACT	18. NUMBER OF PAGES	19a. NAME OF RESPONSIBLE PERSON
a. REPORT	b. ABSTRACT	c. THIS PAGE			Justin R. Bickford
Unclassified	Unclassified	Unclassified	UU	26	19b. TELEPHONE NUMBER (*Include area code*) (301) 394-5127

Contents

List of Figures

Acknowledgments

This work was supported by the Research and Development Engineering Command's (RDECOM) Kinetic Energy Active Protective System (KEAPS) and Photonic Infrared Cueing System (PICS) programs. Thanks go to the KEAPS and PICS development teams for their support during this investigation.

INTENTIONALLY LEFT BLANK.

Summary

Uncooled mid-infrared photoconductors are used in situations where hot objects (such as fire, explosions, engines, etc.) need to be detected using compact, low-cost systems. We have experienced trouble obtaining reliable detector data from mid-infrared photoconductor vendors. The purpose of this report is to give a detailed discussion of how to characterize the signal and noise properties of photodetectors with an emphasis on avoiding the measurement pitfalls associated specifically with room temperature and near room temperature mid-infrared photoconductors. The report ends with a discussion of where it is appropriate to use a commonly used figure of merit.

1. Introduction

Room-temperature (RT) and near-RT mid-infrared (MIR) photoconductors are being used in several heat detection systems that require fast, compact, cheap, non-cryogenic operation. These systems provide a compact means of detecting hot objects (fire, explosions, engines, etc.) that have substantial MIR emissions. In contrast, warm objects (humans, animals, etc.) that have substantial long-infrared emissions are typically sensed with systems based on mercury cadmium telluride (HgCdTe) and quantum well infrared photodetector (QWIP) technologies, which require cryogenic equipment. Figure 1 shows an example of a rectangular MIR lead selenide (PbSe) detector for use at or near RT.

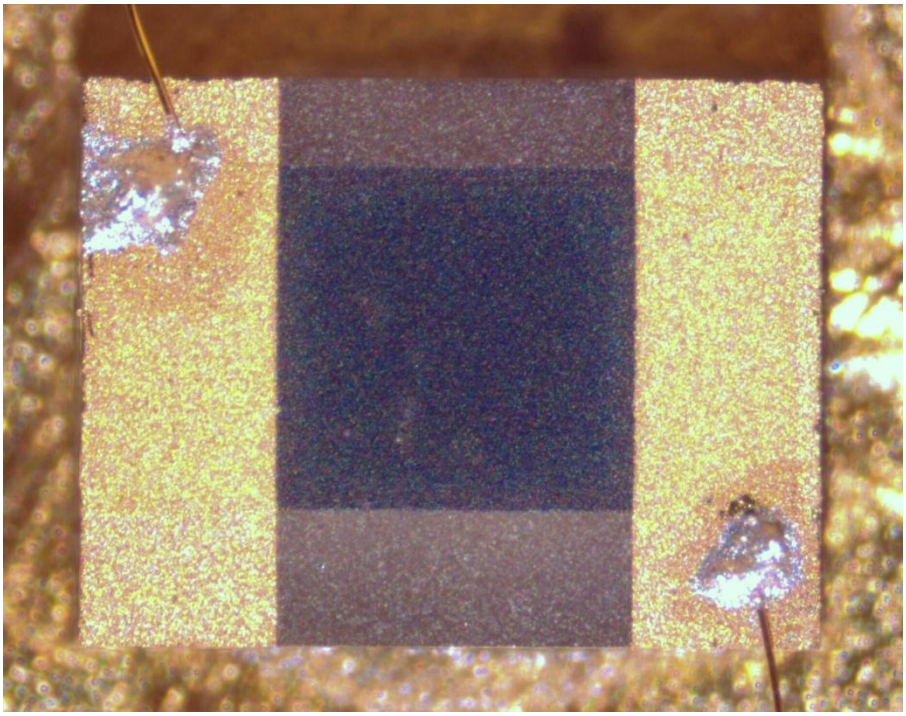

Figure 1. MIR PbSe detector example.

We have witnessed major detector manufacturers get sloppy in their photoconductor analysis. There are several pitfalls that must be addressed to accurately analyze signal and noise measurements. Special attention must be paid to the characterization of RT and near-RT MIR photoconductors, as there are several measurement equipment nuances that are not apparent when measuring cold photovoltaic or cold photoconductive detectors.

This report describes our experience in characterizing these types of detectors. It includes detailed descriptions of radiometry calculations, measurement pitfalls, noise analysis, and

concludes with a discussion of the pitfalls of a common IR detector figure of merit. Much of the analysis presented in this report follows that set forth in reference 1.

2. Methods, Assumptions, and Procedures

2.1 Responsivity Characterization

2.1.1 Responsivity Measurement Experimental Setup

The final responsivity measurement setup is shown in figure 2. The Keithley 2400 Sourcemeter is provides a bias voltage to the detector and measures its bias current. The detector is inside an electrically and cold shielded Dewar. Note that the bias leads, detector, and signal leads remain electrically shielded from the source to the amplifier. The detector is separated from the blackbody by a known distance, the blackbody opening is chopped by a RT chopper, and the chopper output is passed through a RT aperture. The EG&G 5210 lock-in amplifier (5210) has its internal 10^6 V/A transimpedance amplifier (TIA) engaged. This TIA has an input impedance of only ~250 ohms, so the 5210 is effectively measuring the detector's short-circuit root mean squared (rms) current signal. The 5210 can accommodate a bias current of up to 14.1 µA in this configuration, so this method is useful for high resistance photocurrent detectors (as is typically the case at or near RT). The bandwidth of the internal 10^6 V/A TIA is 60 kHz, which is more than adequate for most detector measurement demands.

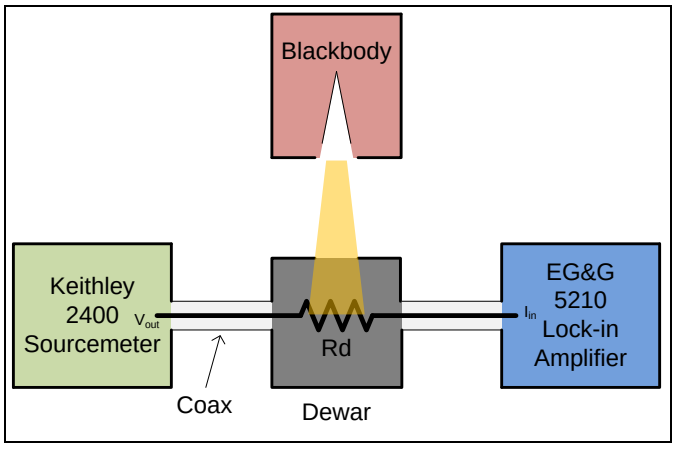

Figure 2. Responsivity measurement setup illustration.

An alternative method is to apply a bias current and measure the open circuit signal voltage. This becomes necessary when measuring lower resistance detectors due to the TIA's bias current accommodation. However, when measuring signal voltage, the 5210's input capacitance presents an RC bandwidth limit to the measurement.

The circuit associated with the first case of voltage bias and current signal measurement is illustrated in the schematic of figure 3. Figure 3a shows the DC circuit, while figure 3b shows the AC equivalent circuit. The DC circuit's capacitor is shorted by the TIA's internal virtual short and does not show up in the AC circuit. Its associated peak-to-peak photocurrent signal is described by equation 1 and is flat with frequency within the bandwidth of the TIA.

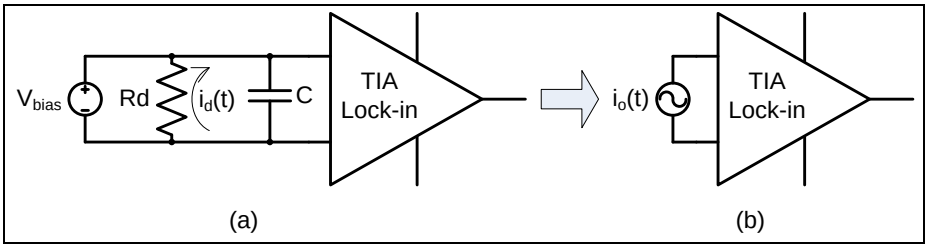

Figure 3. Case 1: schematics showing the (a) DC voltage bias with current signal measurement circuit and the (b) resulting AC equivalent.

$$i_o = i_{ph} \tag{1}$$

The circuit associated with the second case of current bias and voltage signal measurement is illustrated in the schematic of figure 4. Figure 4a shows the DC circuit, while figure 4b shows the AC equivalent circuit. The DC circuit's capacitor is no longer shorted by the lock-in in voltage measurement mode and does not get removed in the AC circuit. Its associated peak-to-peak signal voltage is described by equation 2 and presents a standard RC rolloff frequency spectrum, which becomes pronounced as R_d increases. The capacitance is dominated by lead and lock-in input capacitances as is discussed in section 2.2.2.

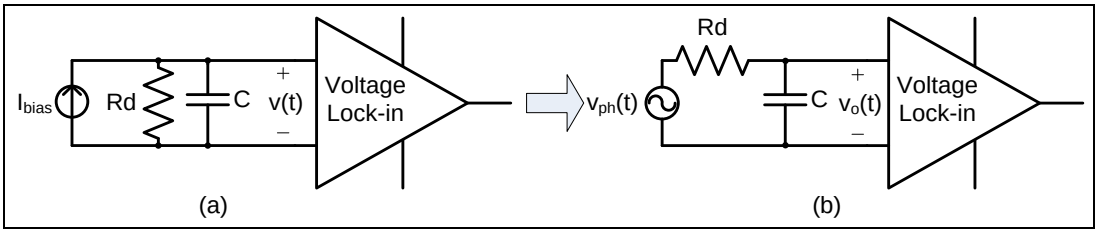

Figure 4. Case 2: schematics showing the (a) DC current bias with voltage signal measurement circuit and the (b) resulting AC equivalent.

$$v_o = \frac{i_{ph} R_d}{1+(\omega R_d C)^2} \tag{2}$$

The blackbody's chopper blocks the light coming out of the aperture periodically. The resulting intensity on the detector is not a perfect square wave due to the circular shape of the aperture and the radial shape of the chopper blades. The peak-to-peak value is of use when analyzing detector properties; however, the lock-in amplifier collects fundamental frequency rms values. The ratio of the fundamental rms component to the peak-to-peak value changes with aperture diameter according to equation 3.56 found in reference 1 and is called the chopper's modulation factor C_{mf}. Equation 3 shows the proper use of the modulation factor. Section 2.1.2 deals with peak-to-

peak data; however, when generating signal-to-noise ratios (SNR) the signal should be in rms to match the rms form of noise.

$$i_{o\,pp} = \frac{i_{o\,rms}}{C_{mf}} \tag{3}$$

2.1.2 Responsivity Radiometry Analysis

This section describes the radiometry analysis necessary to interpret measurement results. The following equations deal with peak-to-peak values. The modulation factor must be implemented when generating responsivity values from these calculations and signal measurements. Exitance is defined as the power per aperture area exiting the blackbody. This is a measure of the light being emitted by the blackbody into a half-space hemisphere and is in units of either W/m for radiant exitance or (photons/s)/m^2 for photon exitance. Radiant exitance (equation 4) is generally useful for system designers, while photon exitance (equation 5) is more relevant to detector analysis. Equations 4 and 5 describe the total exitance, which is the sum of all wavelength contributions and is the most basic exitance that can be used to describe a blackbody. T_s and T_d are the source and detector temperatures in Kelvin, $\bar{\varepsilon}$ is the average spectral emissivity, and sigma is the Stefan-Boltzmann constant (which is approximately 1.52x10^{11} photons/ ($s{\cdot}cm^{2}{\cdot}K^{3}$) or 5.67x$10^{-12}$ W/($cm^{2}{\cdot}K^{4}$)).

$$M_r = \sigma_r \bar{\varepsilon}(T_s^4 - T_d^4) \tag{4}$$

$$M_q = \sigma_q \bar{\varepsilon}(T_s^3 - T_d^3) \tag{5}$$

Solid angle is an angular measure of the field of view of the detector and is in units of steradians. True solid angle refers to the projection of a point source onto a spherical surface or vice versa; however, the more useful version for practical radiometry analysis is that of the projected solid angle, which accounts for the planar nature of commonly found sources. To illustrate this point, consider the solid angle between a point and a hemisphere, the true solid angle would be 2π, while the projected solid angle would be π. During testing, we generally deal with flat circular blackbody apertures and small flat detectors. The projected solid angle for an aperture of radius *r* set a distance *R* away is described by equation 6. It assumes that the aperture and detector are parallel; any angle between them would require a more general analysis.

$$\Omega = \pi \frac{r^2}{R^2 + r^2} \tag{6}$$

Irradiance describes the power receivable by a detector's area. It is described by equation 7 and is in units of either W/m^2 or (photons/s)/m^2. The SI recognized symbol for irradiance is E, but F is used here to avoid confusion with electric field.

$$F = M\frac{\Omega}{\pi} \tag{7}$$

The detector's input optical power is defined by equation 8, where *w* and *l* are the width and length of the detector, respectively.

$$P = F_r wl \tag{8}$$

Responsivity is typically reported in either V/W or A/W as shown in equation 9, which is useful to a system designer, as they typically work with radiant quantities like watts and either current or voltage. However, this definition is not bias independent and it is typically reported at an optimum bias point, which the system designer may or may not be able to use.

$$\mathcal{R}_{A/W} = \frac{i_{ph}}{P} \tag{9}$$

Photoconductors generate current according to equation 10, where *n* is the density of carriers that are collected by the contacts, υ is the carrier drift velocity, *q* is the electron charge, and *h* and *w* are the detector's height and width, respectively (assuming the detector's contacts are in the *h*x*w* plane). When the carriers are thermally generated, this equation describes the photoconductor's dark current. When the carriers are photogenerated, this equation describes the photocurrent. A variant of the same equation is used to derive the generation-recombination noise current.

$$i = \text{nυqhw} \tag{10}$$

The carrier generation rate (equation 11) is the number of available photons arriving on the detector that are converted to electron-hole pairs. This conversion efficiency is called quantum efficiency η.

$$\dot{N} = \eta F_q wl \tag{11}$$

Only a certain number of these carriers will reach the contacts due to their lifetime τ, which is a natural consequence of carrier scattering and annihilation at defects within the photoconductive material. To obtain the collected photogenerated carriers density, we must divide the number of collected carriers by the volume of the detector as shown in equation 12.

$$n = \frac{\dot{N}\tau}{hwl} = \frac{\eta\tau F_q}{h} \tag{12}$$

Carrier drift velocity is defined by equation 13, where *E* is electric field, μ is the average carrier mobility (not the material's permeability), and V_d is detector bias voltage.

$$\upsilon = \mu E = \frac{\mu V_d}{l} \tag{13}$$

Equations 12 and 13 can be substituted into equation 10 to obtain the photocurrent shown in equation 14.

$$i_{ph} = \eta\tau\mu q F_q \frac{w}{l} \tag{14}$$

2.2 Noise Characterization

2.2.1 Noise Measurement Experimental Setup

The final noise measurement setup is illustrated in figure 5. We arrived at this series resistor and lock-in amplifier configuration after testing multiple other schemes. The traditional method of measuring MIR detector noise is to use a TIA with the ability to both apply a bias voltage to the detector as well as cancel out this bias when outputting its amplified voltage. A common instrument to use is the Keithley 428 TIA. We tried using a Keithley 428, a DL Instruments 1212 TIA, and an EG&G 5210 (with internal TIA preamplifier) and experienced trouble with all three. The 428 has the ability to apply a bias voltage to the detector and a DC current suppression circuit to prevent its TIA from being overloaded with DC current. This circuit automatically inserts resistors to accomplish this, which add not only thermal noise, but 1/f noise (because they are biased). We were able to calculate and remove a large portion of this excess noise by assuming it was thermal noise dominant, but the 1/f noise component could never fully be accounted for. The effect shows up noticeably when one tests detectors across various bias levels as different current suppression resistors are inserted. The 1212, 428, and 5210 all showed variations in detector noise even under zero bias (i.e., thermal noise) depending on which TIA gain setting was chosen, despite extracting the noise from the TIA feedback resistors. The errors ranged between 20% and 50%. We believe the issue was due to not correctly accounting for the input impedance and frequency response of the TIAs at each gain setting. The TIA method also suffers simply from the fact that they measure noise current. The measured noise current must be distinguishable from its own internal noise, which is difficult to accomplish with near-RT and RT photoconductive detectors. We were unable to distinguish the thermal noise of detectors above ~1 Mohm from each amplifier's own open circuit noise.

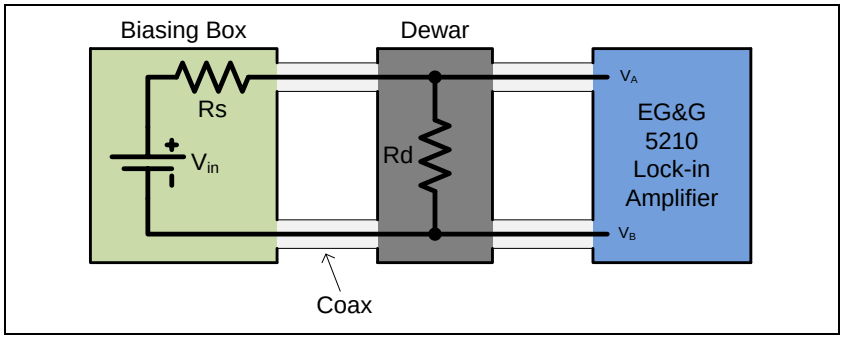

Figure 5. Noise measurement setup illustration.

The situation is significantly different for photovoltaic detectors, as their thermal noise is quite low (they are typically operated at low temperature) and their effective output impedance is extremely high (~Gohms), easily swamping even the TIA's highest input impedance. Being diodes, they also do not present much DC current, which lowers their current suppression circuit noise. The TIA method is a viable noise measurement scheme, we simply were unable to resolve

near-RT photoconductor noise components to within ~50% of expected values using any available TIAs.

In an attempt to improve the noise resolution, we investigated the loaded noise voltage measurement setup shown in figure 5. V_{in} is the DC-bias source, which in our case is a set of AA sized alkaline batteries. These were chosen to conservatively avoid bias circuit noise. The series resistor Rs serves to both DC-bias the detector Rd as well as prevent the detector noise voltage from being shunted. The 5210's differential voltage input mode was chosen to improve noise measurement stability and lower cable capacitance. Unfortunately, this setup does suffer from a low RC limit, but at least the noise spectrum below the RC limit is not hampered by odd TIA spectrally dependent gain. The 5210 has line rejection filters, but their bandwidth is large, deteriorating the noise spectrum at low frequency. We were able to extract near-RT and RT photoconductor detector noise terms within ~5–10% for detector resistances from ~50 ohms to ~30 Mohms using the method described below.

The 5210 measures noise voltage by effectively rectifying the noise within a very well-defined equivalent noise bandwidth (ENBW) using equation 15. This equation is explained in the 5210's user manual. The *percent of full range* value is the output of the 5210, the *full range* value describes the amplifier gain, and the constant converts the sinusoidal detected noise signal into an rms Gaussian noise term. The result is the rms spectral noise voltage v_n.

$$v_n = \frac{1.2214(percent\ of\ full\ range)(full\ range)}{\sqrt{ENBW}} \tag{15}$$

2.2.2 Noise Circuit Analysis

Figure 6 shows a generalized circuit schematic depicting our idealized noise measurement setup. V_o^+ and V_o^- are connection points to the lock-in amplifier front end.

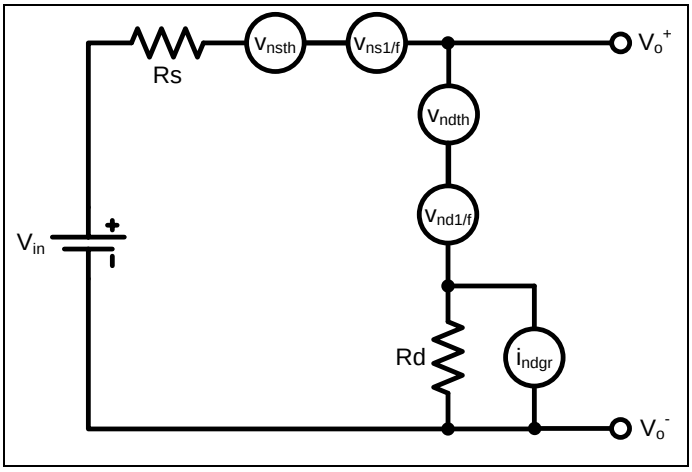

Figure 6. Idealized noise measurement circuit schematic.

Both the series resistor and the detector act as resistors and contribute thermal noise governed by equation 16. This noise term is independent of bias and is constant over all frequencies, i.e., a "white noise" source.

$$v_{nth} = \sqrt{4kTR} \tag{16}$$

Both resistors also contribute 1/f noise, which is described by equation 17, where *A* is a 1/f noise coefficient specific to each device. The *A* coefficient is comparable across related material types, but inherently different for every device. The 1/f name describes the frequency behavior of the v^2 power spectral density, not the noise voltage spectral density. For circuit analysis, it is easier to deal with voltages and currents, while during measurement it is easier to deal with the square of these. 1/f noise is typically attributed to charge carrier scattering within the host material by crystal boundaries and defects and is an ensemble effect. Each scattering center acts as a trap with an associated carrier lifetime and their sum typically results in an approximate 1/f spectrum. While the behavior does not follow an exact 1/f spectrum in practice, it is simpler to work with an idealized equation. Carrier scattering is related to drift velocity, which is why equation 2 is a function of bias. It is important to choose series resistors with low 1/f noise to prevent swamping out the 1/f noise of the detector. The series resistor should also be of high resistance, comparable to the detector's resistance to extract detector noise accurately. These two constraints of requiring high resistance and low 1/f noise typically dictate the use of wire wound resistors for the series resistor. Low inductance wound resistors should be chosen to reduce frequency analysis complications.

$$v_{n1/f} = A\frac{v_{dc}}{\sqrt{f}} \tag{17}$$

If the detector is illuminated with a photon irradiance of *Fq*, it will generate a nonzero generation-recombination noise current described by equation 18. However, the illumination applied must generate a carrier density that is noticeable in comparison to the steady-state dark carrier density for the effect to be seen. This is difficult to achieve at near RT.

$$i_{ngr} = \sqrt{4\eta F_q wl}\frac{\tau\mu q V_{\mathrm{dc}}}{l^2} \tag{18}$$

A few key assumptions have been made in arriving at the schematic shown in figure 6. The DC-bias battery source's internal series resistance and its associated noise have been ignored because their contribution is negligible. All of the reactive components associated with series resistor and detector capacitance as well as lead inductance and capacitance have been ignored for now. Figure 7 illustrates a simplified noise voltage power spectrum (a real noise spectrum would have multiple anomalous spikes as well as other spectral measurement artifacts). 1/f noise dominates in the lower frequency range, thermal noise dominates in the midrange, and the system's RC limit dominates in the high range. If the 1/f noise coefficient is large, the DC bias is high, and/or the resistance is large, the RC limit region may overlap the 1/f region and there will be little to no distinguishable white noise region. This is sometimes the case with PbSe photoconductors.

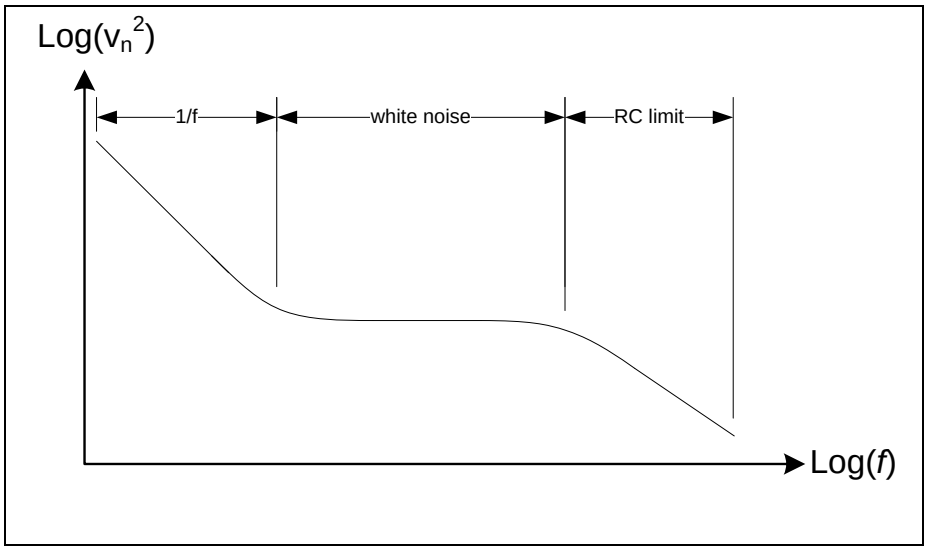

Figure 7. Simplified noise spectrum.

The lock-in amplifier input sees a combination of the series resistor noise together with the detector noise at the circuit output. To definitively separate the noise components, the circuit must be analyzed. To perform the analysis properly, each noise source must be separately transformed between Thevenin and Norton equivalents until they present themselves at the output terminals. All remaining voltage sources must be considered shorts and all remaining current sources must be considered open circuits. Every time a Thevenin equivalent voltage is converted to a Norton equivalent current, the current becomes the Thevenin voltage divided by its associated resistance. Figure 8a–e illustrates how this analysis is done. All of the noise sources have been presented as current noise sources in the final circuit shown in figure 8f. Doing so makes the final noise equation more tractable.

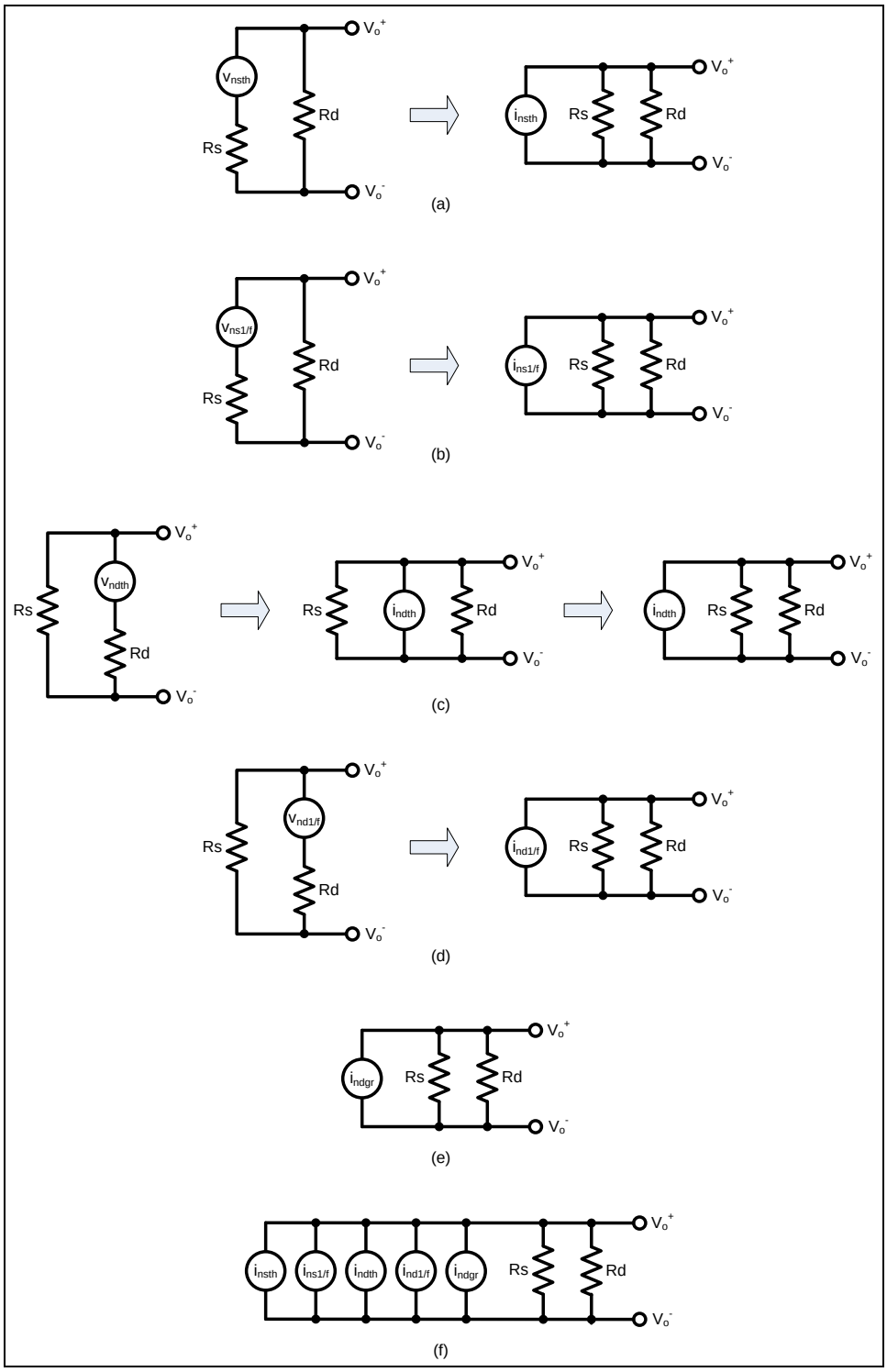

Figure 8. Noise source conversions for (a) Rs thermal noise, (b) Rs 1/f noise, (c) detector thermal noise, (d) detector 1/f noise, (e) detector generation-recombination noise, and (f) final output referred noise circuit.

The final noise current components are as follows:

$$i_{nsth} = \sqrt{\frac{4kT_s}{R_s}} \tag{19}$$

$$i_{ndth} = \sqrt{\frac{4kT_d}{R_d}} \tag{20}$$

$$i_{ns1/f} = \frac{A_s V_s}{R_s\sqrt{f}} = \frac{A_s V_d}{R_d\sqrt{f}} \tag{21}$$

$$i_{nd1/f} = \frac{A_d V_d}{R_d\sqrt{f}} \tag{22}$$

$$i_{ndgr} = \sqrt{4\eta F_q wl}\,\frac{\tau\mu q V_d}{l^2} \tag{23}$$

Since noise sources vary randomly, only their powers may be added. Therefore, all noise sources must be added in quadrature. The lock-in will only be able to see the noise voltage present at the output terminals; this requires that we convert the noise current components in equations 19–23 to the total output noise voltage shown in equation 24. It is simpler to deal with the square of the noise voltage during measurement analysis, so this convention is presented in equation 24.

$$\mathrm{v}^2_{\mathrm{ntotal}} = \underbrace{\left(\frac{R_s R_d}{R_s + R_d}\right)^2}_{\text{Rs||Rd}} \left(\underbrace{\frac{4kT_s}{R_s} + \frac{4kT_d}{R_d}}_{\text{thermal components}} + \left(\underbrace{\left(\frac{A_s^2}{R_d^2} + \frac{A_d^2}{R_d^2}\right)\frac{1}{f}}_{\text{1/f components}} + \underbrace{4\eta F_q wl\,\frac{\tau^2\mu^2\mathrm{q}^2}{l^4}}_{\text{gen/rec component}} \right) v_d^2 \right) \tag{24}$$

The first term in equation 24 is the parallel combination of the series and detector resistances. Typically, this combination would be small in comparison to the input resistance of the lock-in; however, PbSe devices can have large resistances. If this parallel resistance is larger than about 10% of the input resistance, this term should be replaced with the parallel combination of all three resistances.

Note that equation 24 does not include the RC limit phenomenon shown in figure 7. The dominating capacitances will be from the leads, and lock-in input capacitance, which are both in parallel with the lock-in input. An RC rolloff term like that of equation 2 would have to be applied to equation 24 to fully describe the noise voltage measured by the lock-in amplifier. Standard 1–2 μm thick PbSe square photoconductors should have capacitances below ~1 fF. Carefully chosen series resistors should have capacitances below a few pF. A half meter of common RG-58/U 50 ohm coaxial cable should contribute ~40 pF, while the lock-in may contribute ~25 pF. Additional lead capacitances within the Dewar could bring the total to ~80 pF. A series resistor of ~5 Mohms (which will dominate the parallel combination) combined with this 80-pF capacitance will yield an RC corner frequency of only ~400 Hz.

By measuring the noise at various frequencies and varying the detector's bias, a series of spectral trendlines can be obtained. From these trends each noise component can be extracted and the expected noise behavior of the detector acting on its own can be realized. Any deviation in these trends should be considered a measurement error that must be investigated. Because the 1/f noise stems from material defect density, and resistance and responsivity dictate the signal, signal and noise characterization provides valuable feedback to device fabricators and system designers.

3. Results and Discussion

One of the most common figures of merit used to judge IR detectors is their specific detectivity *D**, it allows system designers to determine their SNR in reference to a standardized detector size/shape and test condition. Its definition is given by equation 25, where $\mathcal{R}_{V/W}$ is the open circuit responsivity in V/W, A is the photon capturing area of the detector, v_n is rms noise voltage, and f_{bw} is the measurement bandwidth.

$$\mathrm{D}^* = \frac{\mathcal{R}_{V/W}\sqrt{A}}{v_n/\sqrt{f_{bw}}} \tag{25}$$

It does not, however generally provide a fundamental material figure of merit, and therefore, cannot be used to compare materials fabricated by different manufactures without consideration to test conditions. *D** can only be used to compare device performance between similar test and applications scenarios. Although most manufacturers try to stay above the 1/f noise region while measuring *D**, the result may not be a good predictor of system performance if the device is used under different conditions. Using *D** to compare different materials systems should also be discouraged. Many manufacturers will publish background limited infrared photon *(BLIP) D** by lowering the temperature of the device to the point where generation recombination noise dominates over thermal noise. Equation 26 describes *D** for photoconductors ignoring the influence of 1/f noise and system RC bandwidth. E is the detector's bias electric field, η is its quantum efficiency, h is the material height (not Planck's constant), and F_q is the photon irradiance.

$$\mathrm{D}^* = \frac{\eta\mu\tau q E}{\sqrt{4\eta F_q q^2(\tau\mu E)^2 + \frac{4kTh}{\rho}}} \tag{26}$$

The two terms in the denominator are the generation-recombination noise and thermal noise. In the BLIP limit the thermal noise contribution is negligible and the *D** collapses to equation 27. From which quantum efficiency can be calculated if F_q is known. Quantum efficiency is related to absorption depth and thickness, so it is a good indicator of detector performance, but should not be used to compare materials of different thickness. Assuming a comparable thickness

across devices, this is an ideal material comparison figure of merit if the device is to be used in the BLIP regime.

$$D^*_{BLIP} = \frac{\eta\mu\tau qE}{\sqrt{4\eta F_q q^2(\tau\mu E)^2}} = \sqrt{\frac{\eta}{4F}} \tag{27}$$

If the system requirements dictate working at RT, which is often well beyond the BLIP limit, *D** becomes equation 28. In this temperature limited (TL) regime, the result is both temperature and bias dependent. The temperature dependence stems from the *T* in the denominator as well as ρ. Caution is advised when *D** is used to compare devices operating in this regime.

$$D^*_{TL} = \eta\mu\tau qE\sqrt{\frac{\rho}{4kTh}} \tag{28}$$

4. Conclusions

We have presented a detailed discussion of how to characterize the signal and noise properties of RT and near-RT MIR photoconductors. We have also described our measurement methods and how we arrived at these methods. We are routinely able to measure self consistent signal and noise values to within a few percent repeatability using the techniques described in this report; this is no simple task with noise measurements. We generated this report after experiencing a lot of difficulty conveying how to properly measure these types of detectors to coworkers and outside professionals.

Unfortunately, for near-RT photoconductor-based systems, there is no catch-all figure of merit and it is best to test individual devices for use in systems and compare them using all available signal and noise data. The alternative is to characterize all of the material constants, such as μ, η, τ, n_{th}, and $A_{1/f}$, and build a device performance model from the ground up. Although this may seem daunting, it is not impossible and it is sometimes necessary.

On a final note, many system designers fall into the trap of comparing *D** between different materials without considering other important factors, such as PC versus PV device performance, wavelength dependence, operating temperature, maximum speed, cost, and manufacturability. As a device researcher, it would be wise to be sure that the system designers one is working with understand the importance of these factors.

5. References

1. Vincent, J. D. *Fundamentals of Infrared Detector Operation & Testing*; Wiley: New York, 1990.

List of Symbols, Abbreviations, and Acronyms

1212	DL Instruments 1212 transimpedance amplifier
428	Keithley 428 transimpedance amplifier
5210	EG&G 5210 lock-in amplifier
BLIP	background limited infrared photon regime
D*	specific detectivity
HgCdTe	mercury cadmium telluride
KEAPS	Kinetic Energy Active Protective System
Lock-in	lock-in amplifier
MIR	mid-infrared (3–5 μm wavelengths)
PbSe	lead selenide (a photoconductor material)
PC	photoconductor
PIC	Photonic Infrared Cueing System
PV	photovoltaic
QWIP	quantum well infrared photodetector
RDECOM	Research and Development Engineering Command
rms	root mean squared
SNR	signal to noise ratio
TIA	transimpedance amplifier
TL	temperature limited regime

NO. OF COPIES	ORGANIZATION
1 PDF	DEFENSE TECH INFO CTR ATTN DTIC OCA 8725 JOHN J KINGMAN RD STE 0944 FT BELVOIR VA 22060-6218
1	US ARMY ARDEC ATTN RDAR MEF F N CALI BLDG 59 PICATINNY ARSENAL NJ 07806-5000
1	US ARMY CERDEC ATTN RDER IWE SF C KAISER ABERDEEN PROVING GROUND MD 21005
1	US ARMY CERDEC ATTN RDER IWE SF W MOLONEY ABERDEEN PROVING GROUND MD 21005
9 HCS	US ARMY RSRCH LAB ATTN IMAL HRA MAIL & RECORDS MGMT ATTN RDRL CIO LL TECHL LIB ATTN RDRL CIO LT TECHL PUB ATTN RDRL SEE E J BICKFORD ATTN RDRL SEE E P PELLEGRINO ATTN RDRL SEE E N BAMBHA ATTN RDRL SEE E W CHANG ATTN RDRL SEE G WOOD ATTN RDRL SEE P GILLESPIE ADELPHI MD 20783-1197
TOTAL:	13 (12 HCS, 1 PDF)

INTENTIONALLY LEFT BLANK.